



## Research Article

Theme: Modeling and Simulations of Drug Product Manufacturing Unit Operations  
Guest Editors: Alexander Russell and Maxx Capece

# A Software Tool for Lyophilization Primary Drying Process Development and Scale-up Including Process Heterogeneity, I: Laboratory-Scale Model Testing

Robin Bogner,<sup>1</sup> Emily Gong,<sup>2,7</sup> William Kessler,<sup>2</sup> Michael Hinds,<sup>2</sup> Arushi Manchanda,<sup>1</sup> Seongkyu Yoon,<sup>3</sup> Huolong Liu,<sup>3</sup> Richard Marx,<sup>3</sup> Jessie Zhao,<sup>4</sup> Puneet Sharma,<sup>4</sup> Akhilesh Bhambhani,<sup>5</sup> Justin Stanbro,<sup>5</sup> Alina Alexeenko,<sup>6</sup> and Petr Kazarin<sup>6</sup>

Received 25 May 2021; accepted 1 September 2021; published online 12 November 2021

**Abstract.** Freeze-drying is a deceptively complex operation requiring sophisticated design of a robust and efficient process that includes understanding and planning for heterogeneity across the batch and shifts in parameters due to vial or lyophilizer changes. A software tool has been designed to assist in process development and scale-up based on a model that includes consideration of the process heterogeneity. Two drug formulations were used to test the ability of the new tool to develop a freeze-drying cycle and correctly predict product temperatures and drying times. Model inputs were determined experimentally, and the primary drying heterogeneous freeze-drying model was used to design drying cycles that provided data to verify the accuracy of model-predicted product temperature and primary drying time. When model inputs were accurate, model-predicted primary drying times were within 0.1 to 15.9% of experimentally measured values, and product temperature accuracy was between 0.2 and 1.2°C for three vial locations, center, inner edge, and outer edge. However, for some drying cycles, differences in vial heat transfer coefficients due to changes in shelf and product temperature as well as altered product resistance due to product temperature-dependent microcollapse increased inaccuracy (up to 28.6% difference in primary drying time and 5.1°C difference in product temperature). This highlights the need for careful determination of experimental conditions used to calculate model inputs. In future efforts, full characterization of location- and shelf temperature-dependent  $K_v$ , as well as location- and product temperature-dependent  $R_p$ , will enhance the accuracy of the predictions by the model within the user-friendly software.

**KEY WORDS:** heterogeneous freeze-drying; process model; TDLAS; microcollapse.

## INTRODUCTION

Many pharmaceuticals (approximately 30–50%), particularly “biotechnology products,” do not have sufficient chemical and physical stability to withstand the rigors of

distribution and storage in aqueous solution, so conversion to a stable solid is essential (1). Lyophilization, also known as freeze-drying, is a process by which a dry solid is produced from a solution, normally aqueous, by first converting most of the solvent to solid (ice), removal of the ice by sublimation, and finally, removal of any unfrozen water by desorption (2, 3). Freeze-drying is an expensive process because process times are long and commercial freeze-drying plants are very expensive to purchase and maintain, motivating the development of efficient cycles that produce high-quality drug product for all vials dried within the lyophilizer.

During lyophilization, a careful balance of heat into the product and sublimation heat flux out of the product is required to maintain the product below its critical temperature. During primary drying, the shelf temperature and drying chamber pressure are controlled, but the product temperature is not directly controlled and is lower than the shelf temperature. Due to the low pressure required to remove

<sup>1</sup> Department of Pharmaceutical Sciences, University of Connecticut, Storrs, CT, USA.

<sup>2</sup> Physical Sciences Inc., 20 New England Business Center, Andover, MA, USA.

<sup>3</sup> Department of Chemical Engineering, University of Massachusetts Lowell, Lowell, MA, USA.

<sup>4</sup> Genentech, South San Francisco, California, USA.

<sup>5</sup> Merck, West Point, PA, USA.

<sup>6</sup> Davidson School of Chemical Engineering, Purdue University, West Lafayette, Indiana, USA.

<sup>7</sup> To whom correspondence should be addressed. (e-mail: egong@psicorp.com)

water (typ. 30–200 mTorr, 4–25 Pa), there is a high resistance to heat transfer from the shelf to the product.

Many small innovative companies are pursuing the development of biopharmaceuticals and vaccines, which are often labile in solution, requiring stabilization by lyophilization for storage and distribution before administration to the patient. However, there is a worldwide shortage of scientists and engineers that have the required understanding of freeze-drying to develop robust, optimized process cycles that assure product quality while achieving process efficiency. Cycle development by inexperienced engineers often results in inefficient (costly) cycles, failures in scale-up or technology transfer, and poor (heterogeneous) product quality, which can confound clinical trials and product performance. A lack of freeze-drying experience also hinders interactions with and oversight of contract manufacturers. Development of easy to use or automated process development tools can help fill the gap between need and expertise.

Freeze-drying is a deceptively complex operation (4–7) requiring sophisticated design of a robust and efficient process (Fig. 1). Largely because of the complexity and the lack of adequate process analytical technology, most commercial freeze-drying processes are sub-optimal, thereby wasting time and/or placing product quality at risk. Both measurement and control of product temperature and timing of the change in shelf temperature from primary to secondary drying conditions are critical (8–10). In many cases, processes optimized to maintain the product below a critical temperature at lab-scale cannot be simply transferred to sterile manufacturing because of changes in vial heat transfer rates, ice nucleation temperatures and ice crystal growth rates that affect ice microscopic structure, and lyophilizer mass and/or heat transfer overload limits (11). The product temperature during freeze-drying is directly related to water sublimation and desorption rates.

The driving force for sublimation is the difference between the chamber pressure and the vapor pressure of ice at the temperature of the product sublimation interface ( $T_p$ ). Thus, the duration of primary drying (*i.e.*, the ice sublimation stage) is very sensitive to the product temperature. Knowledge of the temperature at which the product undergoes collapse or eutectic melt of the porous structure created during sublimation, denoted the “collapse temperature” ( $T_c$ ) for amorphous formulations, is an important process design parameter.  $T_c$  is the maximum allowable temperature during primary drying (11–14), although recently more companies are beginning to develop and operate cycles with the product temperature exceeding  $T_c$  (14–16). In this publication, experimental results focus on amorphous products, so the focus will be on the collapse temperature. Above the glass transition temperature of the maximally freeze-concentrated solution,  $T_g'$ , during primary drying, the amorphous (typical for biotechnology drugs) freeze-dried cake begins to experience viscous flow, initially resulting in product microcollapse, a consolidation of smaller pores into larger pores. As the product temperature continues to rise, microcollapse may lead to additional loss of the porous structure as it “collapses” into a smaller denser mass that may be unacceptable in a pharmaceutical product from the viewpoints of the customer, the FDA, and the manufacturer. Among other consequences of macrocollapse into a dense mass, perhaps the most serious

is the potential for high residual moisture in the final product, which can increase degradation by-products. Prolonged reconstitution time, caused by collapse, can be serious when the product is self-administered or in an emergency situation (16). Freeze-drying below  $T_c$  is typically necessary to manufacture high quality products with reproducible product performance, although some level of microcollapse is now becoming acceptable if product quality is not adversely affected. Since a 1°C increase in product temperature during primary drying can result in 13% reduction in primary drying time (17), it is of interest to maximize the product temperature during primary drying such that all vials in the batch are close to (but not exceeding)  $T_c$ , thereby motivating accurate  $T_c$  measurements and accurate process control.

Numerous heat and mass transfer models, and freeze-drying process development algorithms (18–21) have been developed to assist scientists and engineers in cycle development. Knowledge and design spaces defined using the steady-state heat and mass transfer equations as described by Patel and Pikal (7) were first reported by Chang and Fisher (5), and its application demonstrated by additional groups (6). A well-accepted approach for generating a process design space based on batch average parameters has been thoroughly discussed in the literature (22, 23). Figure 1 shows a graph of the average sublimation rate as a function of chamber pressure ( $P_c$ ) used to construct the batch-average knowledge and design spaces for the primary drying stage of freeze-drying. Typically five steps are carried out to create the knowledge and design space:

- I. Measure the product formulation collapse or eutectic melt temperature below which the product must be maintained during primary drying.
- II. Establish the relationship between process variables the user can control, freeze-dryer shelf temperature and drying chamber pressure ( $T_s$  and  $P_c$ ) and the key product quality parameter not controlled, product temperature at the sublimation interface,  $T_p$ .
- III. Calculate the sublimation rate vs chamber pressure for shelf temperature isotherms and product temperature isotherms using steady-state heat and mass transfer theory.
- IV. Experimentally determine the lyophilizer equipment capability limit (24).
- V. Graph the process knowledge space and define the process design space (Fig. 1).

The design space is bound by the lyophilizer equipment capability limit and the target product temperature (< critical temperature or any other temperature associated with poor product quality).

Unfortunately, most of the models do not account for the inherent heterogeneity in product temperature and drying time that results from freeze-drying process heterogeneity and simply use batch average inputs. Product in center vials generally dries at lower temperatures and slower rates than inner-edge and outer-edge vials. In addition, product in vials located in the corners of the freeze-dryer shelves tend to be the warmest, drying much faster than center, inner-edge and other outer-edge vials. Vial-based pharmaceutical freeze-drying heterogeneity is due to a number of factors including variation in:

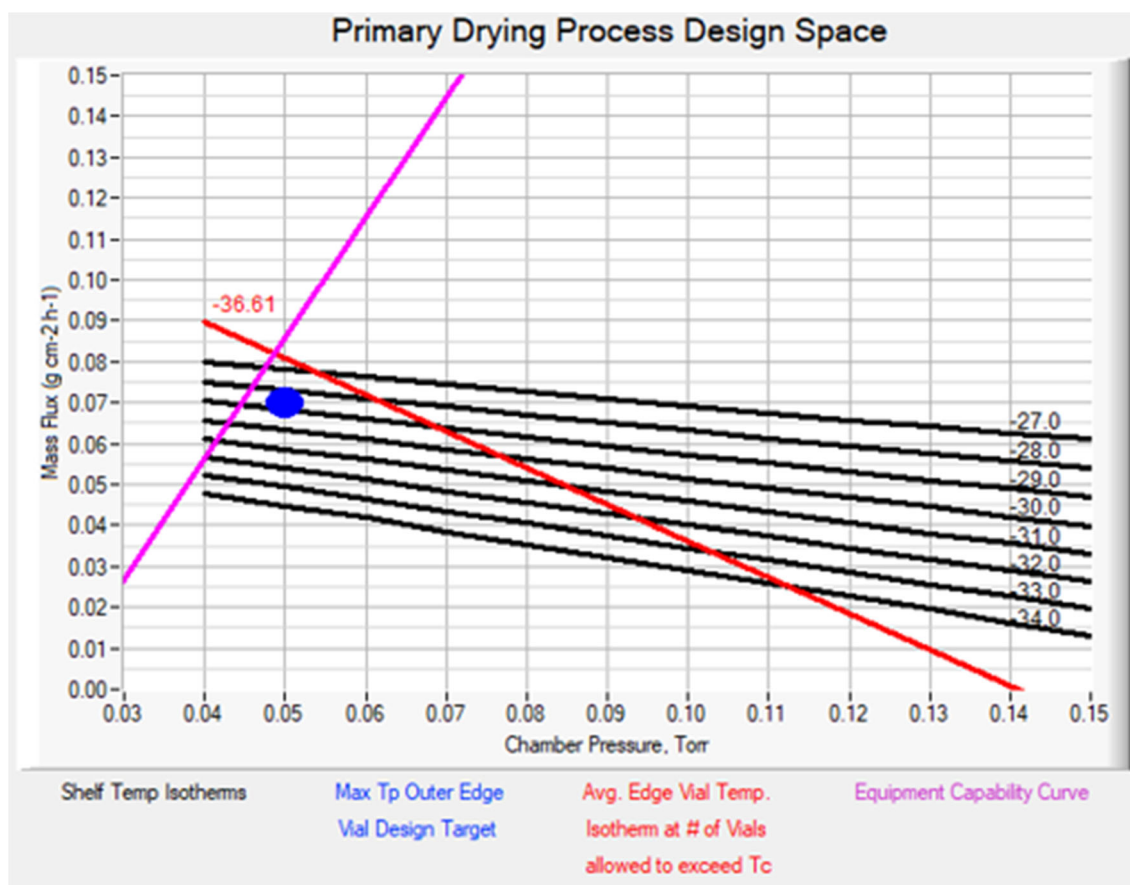


**Fig. 1.** Example lyophilization primary drying process knowledge and design space calculated using the model of heterogeneous freeze-drying. The black lines are shelf temperature isotherms. The red line is the average edge vial temperature for the user-defined number of vials allowed to exceed the critical temperature. The pink line is the equipment capability limit, all plotted as a function of the lyophilizer product chamber operating pressure. The blue dot represents a recommended operating point to maintain outer edge vials below  $T_c$

1. Ice nucleation temperature and ice crystal growth rate resulting in variation in ice structure and resistance to drying,  $R_p$
2. Shelf surface temperature,  $T_s$
3. Heat flux to vials due to location-dependent radiation and gas conduction contributions to  $K_v$ , caused by differences in view factors from vials to the warm lyophilizer chamber walls and door, impacting mostly edge vials
4. The contour of the vial bottom, even in a set of nominally equivalent vials, which influences the gas conduction contribution to  $K_v$
5. Fill volume,  $V_f$

Processes that are developed based on batch-average measurements of  $R_p$ ,  $T_s$ ,  $K_v$ , and  $V_f$  can suffer from collapse of product in the center vials if they fail to complete sublimation before the calculated primary drying time (and a rise in the shelf temperature to the secondary drying setpoint) and/or collapse of product in edge vials if it exceeds the collapse temperature during primary drying. Furthermore, a seemingly successful process may produce collapsed product if there are slight changes in vial manufacturing or during transfer to another lyophilizer. Understanding and planning for heterogeneity across the batch and shifts in parameters due to vial or lyophilizer changes allows the development of a

robust, yet efficient freeze-drying process. The software tool described in this publication is intended to assist in process development and scale-up with consideration of the heterogeneity across the batch.

## MATERIALS AND METHODS

### Model Description

This publication focusses on the development of user-friendly software for lyophilization primary drying process development and experimental testing of the model predictive capability. The software is based on previous work describing the impact of natural variations in freeze-drying parameters on product temperature and drying time and a model for scaling vial heat transfer coefficients from laboratory- to production-scale lyophilizers (25, 26). The previous work described lyophilization process development models based upon the use of Excel spreadsheets. The present effort combined the models into a single algorithm written in C-code to create a user-friendly lyophilization process development and scale-up tool. Following development of the software, data from lab-scale sublimation and freeze-drying runs were used to evaluate the performance of

the model in predicting primary drying time and product temperature according to vial location (center, inner-edge and outer-edge).

The software *Design Space Inputs* and the *Calculation and Results* graphical user interface (GUI) screens are shown in Figs. 2 and 3. The *Design Space Inputs* GUI requires a number of inputs from the end user, including information about the product formulation, container system and fill volume. In addition, the user provides input for the determination of product resistance to drying,  $R_p$ , the vial heat transfer coefficients,  $K_v$ , as a function of chamber operating pressure and vial location, and the lyophilizer equipment capability limits (maximum vapor mass flow *versus* chamber pressure). The authors developed standard operating procedures (SOPs) based on the use of tunable diode laser absorption spectroscopy (TDLAS) (27–31) and gravimetric measurements (32) to guide the user in creating these data sets. In this publication, the authors describe application and testing of the model to address drying heterogeneity. A future publication will describe the process scale-up capability of the software model and the testing of that functionality.

Briefly, the steady-state heat and mass transfer model (18) often used to develop a primary drying process based on batch-average data was extended to describe the heterogeneity in product temperature and drying time across a batch. Three categories of vial locations were identified—center vials (those vials surrounded by 6 vials in a hexagonal closest packing array), inner-edge vials (those vials near the edge that are surrounded by 5 vials), and outer-edge vials (which are at the edge of the array and are surrounded by 3 or 4 vials). The location-dependent  $K_v$  (mean and variance) are model inputs, along with mean and variance for  $T_s$ ,  $V_f$ , and the batch average  $R_p$ . (Future versions of the software will incorporate location dependent values for  $R_p$  and its variance.)

At a constant operating chamber pressure, the first partial derivatives of the maximum product temperature at the bottom center of the vial during primary drying,  $T_{b,max}$ , and primary drying time,  $t_{dry}$ , with respect to each of the parameters,  $K_v$ ,  $T_s$ ,  $V_f$ , and  $R_p$ , are calculated from the ranges in  $T_{b,max}$  and  $t_{dry}$  at  $\pm 10\%$  of the means of  $K_v$ ,  $T_s$ ,  $V_f$ , and  $R_p$ . The partial derivatives along with the corresponding variance of each parameter,  $i$ , ( $\sigma_i^2$ ) are used to calculate the variance of  $T_{b,max}$  ( $\sigma_{T_{b,max}}^2$ ) and of  $t_{dry}$  ( $\sigma_{t_{dry}}^2$ ) for each location class of vials (center, inner-edge, outer-edge) (Eqs. 1 and 2). Distributions of product temperature and drying time are constructed from the mean and variance. The cumulative distributions of product temperature for all vial locations is used to plot the fraction of vials above the maximum product temperature ( $x$ -axis temperature shown in the upper left of Fig. 3) and that of drying time is used to plot fraction of vials containing ice as a function of drying time (upper right plot of Fig. 3).

$$\begin{aligned} \sigma_{T_{b,max}}^2 = & \left( \frac{\partial T_{b,max}}{\partial K_v} \right)_{T_s, V_f, R_p}^2 \cdot \sigma_{K_v}^2 + \left( \frac{\partial T_{b,max}}{\partial R_p} \right)_{T_s, V_f, K_v}^2 \\ & \cdot \sigma_{R_p}^2 + \left( \frac{\partial T_{b,max}}{\partial T_s} \right)_{V_f, R_p, K_v}^2 \cdot \sigma_{T_s}^2 \\ & + \left( \frac{\partial T_{b,max}}{\partial V_f} \right)_{T_s, R_p, K_v}^2 \cdot \sigma_{V_f}^2 \end{aligned} \quad (1)$$

$$\begin{aligned} \sigma_{t_{dry}}^2 = & \left( \frac{\partial t_{dry}}{\partial K_v} \right)_{T_s, V_f, R_p}^2 \cdot \sigma_{K_v}^2 + \left( \frac{\partial t_{dry}}{\partial R_p} \right)_{T_s, V_f, K_v}^2 \cdot \sigma_{R_p}^2 \\ & + \left( \frac{\partial t_{dry}}{\partial T_s} \right)_{V_f, R_p, K_v}^2 \cdot \sigma_{T_s}^2 + \left( \frac{\partial t_{dry}}{\partial V_f} \right)_{T_s, R_p, K_v}^2 \cdot \sigma_{V_f}^2 \end{aligned} \quad (2)$$

Each term in Eqs. 1 and 2 is shown in the table, % contributions to total variance (lower right table in Fig. 3).

Assumptions and approximations:

- The product resistance is treated in this version of the software as location-independent, as are  $V_f$  and  $T_s$ .
- The first partial derivative of  $T_{b,max}$  and  $t_{dry}$  evaluated at  $\pm 10\%$  of the mean of each parameter is assumed to be a good approximation out to 6 standard deviations from the mean.

Figure 3 includes a design space plot of mass flux as a function of the freeze dryer operating pressure. As noted above, the design space is bound by the lyophilizer equipment capability limit and the maximum product temperature, represented by the average edge vial temperature at the number of vials allowed to exceed the collapse temperature. A recommended operating point is defined by the blue dot in Fig. 3, which was calculated using the average outer edge vial product temperature. That temperature defines  $P_{ice}$ , which is used in combination with the chamber pressure and product resistance at the last time point in the model, to calculate the mass flux. The model also predicts the percentage of vials that will undergo collapse and the percentage of vials that have not completed primary drying given a primary drying cycle time. A prior publication used a 5% NaCl/0.2% sucrose formulation to visually assess product collapse and/or meltback (33). Preliminary attempts during this reported work observed variability in the success of using the NaCl/sucrose formulation and were not further pursued.

The software developed based on the model briefly described above and in more detail previously (25, 26) was used to design primary drying cycles for two protein-based drug formulations and test the agreement of location-dependent primary drying times and product temperatures with the model predictions. Due to the small number of thermocouples available to monitor the product in any given lyophilization cycle, it was not yet possible to test agreement of variances.

The authors envisioned that end-users of the model would initially perform a series of experiments to determine the vial location-dependent values of the vial heat transfer coefficient,  $K_v$ , as a function of pressure, the product resistance,  $R_p$ , under conservative drying conditions (to avoid product collapse) and the lyophilizer maximum mass flow rate equipment capability limit. Determination of these parameters in combination with vial container size, formulation solute concentration, formulation fill volume and the collapse temperature would enable use of the software model to develop primary drying cycles and the process knowledge and design spaces over a wide range of conditions. As discussed below, there were limitations to this planned approach requiring a future modification to the suggested process development procedure.



**Fig. 2.** Screen image of the lyophilization primary drying software model user input interface. Inputs include product, container, and lyophilizer equipment capability related parameters. Location- and pressure-dependent vial heat transfer coefficients as well as relative standard deviations for all parameters are required to describe contributors to drying heterogeneity and variation that will affect vial location dependent product temperatures and drying times

**Materials**

Drug formulations were provided by Genentech and Merck. Both formulations contained a protein active

pharmaceutical ingredient and additional cryoprotectants, surfactants, bulking, and buffering agents. The blinded formulations, denoted as formulation A and formulation B, possessed a total solid content of 3.9% w/v and 4.9% w/v,

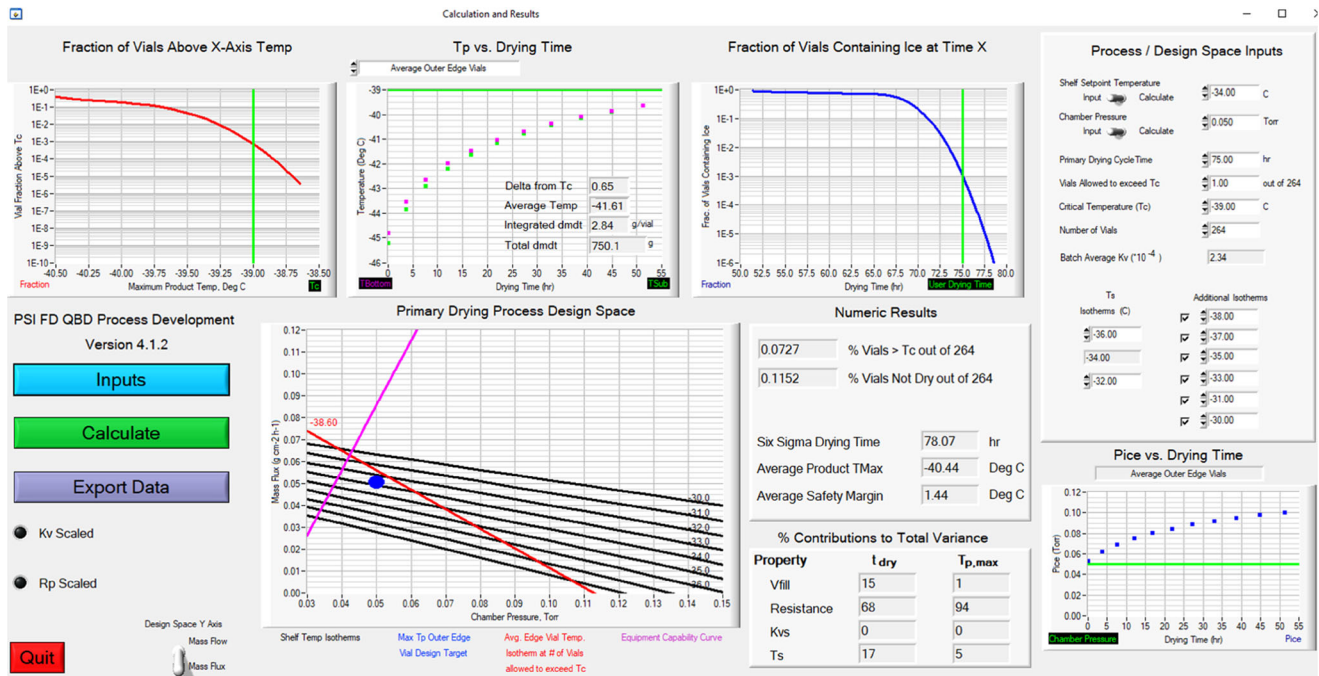


**Fig. 3.** Screen image of the lyophilization primary drying software model output calculations. The outputs include the fraction of vials that dry above the user-defined critical temperature, product location-dependent temperatures, product drying time, percent of vials that collapse, percent of vials that do not complete primary drying, as well as a plot of the process knowledge and design spaces

**Table I.** Measured  $K_v$  values for 10R and 20R vials

Vial	$T_{\text{shelf}}$ (°C)	$P_c$ (mTorr)	$K_v \times 10^4$ (cal/cm <sup>2</sup> /s/K)			
			Center	Inner edge	Outer edge	% $\Delta K_{v,\text{edge}}$
10R Gerresheimer	- 20	60	2.26	2.82	3.4	50
		100	2.71	3.26	3.85	42
		150	3.21	3.92	4.61	44
20R Wheaton	- 20	60	2.77	3.33	4.02	45
		100	3.41	3.94	4.88	43
		150	4.01	4.71	5.54	38
	0	60	2.82	3.18	3.53	25
		100	3.56	4.08	4.37	23
		150	4.57	4.99	5.44	19
	20	60	2.94	3.27	3.65	24
		100	3.72	4.11	4.62	24
		150	4.46	4.93	5.46	22

respectively. Both formulations were amorphous. All solutions were filtered using a 0.22  $\mu\text{m}$  polyethersulfone filter (Thermo Fisher Scientific, Waltham, MA) immediately prior to vial filling. Vials used for  $K_v$  experiments (Table I) were 20R (DWK Life Sciences, formerly Wheaton, Rockwood, TN) and 10R (Gerresheimer, Düsseldorf, Germany) tubing vials. Only 10R vials were used for drug product experiments. Rubber stoppers were 20 mm igloo lyophilization stoppers (Aptar Pharma, Crystal Lake, IL). Data from 20R vials were used to explore the shelf temperature dependence of  $K_v$ . Freeze-drying experiments were conducted using one shelf of filled vials in a LyoStar 3 freeze-dryer (SP Scientific, Gardiner, NY) containing three shelves.

### Freeze Drying

A single, full “bottomless” tray of filled vials was placed on the middle shelf of the lyophilizer. The freeze-dryer was outfitted with a LyoFlux® (Physical Sciences Inc., Andover, MA) tunable diode laser absorption spectroscopy (TDLAS) sensor to measure batch average water vapor mass flow rates during freeze drying. This

data was primarily used to determine batch average  $R_p$  and for developing the equipment capability curve used in the model to develop the knowledge and design spaces. Process settings for determination of the vial heat transfer coefficients ( $K_v$ ) and product resistance ( $R_p$ ) are described in the following two sections.

The primary drying heterogeneous freeze-drying model was used to design experiments that provided data to verify the accuracy of model predictions of product temperature and primary drying time. Freeze-drying for both formulations, A and B, was performed using Gerresheimer 10R vials. The fill volume and depth were 3.0 mL/0.85 cm and 5.2 mL/1.47 cm, respectively, for formulations A and B. The freeze-drying cycle parameters are shown in Table II. Freezing conditions were based on the freezing recipe outlined in Tang et al. (34) for amorphous formulations. The freezing protocol used for both formulations included first lowering the solution temperature to 5°C and holding for 30 min, then lowering the lyophilizer shelf temperature to - 5°C, at a rate of 1°C/min, and holding for 30 min to stabilize the product temperature. The shelf temperature was further lowered at 1°C/min to - 45°C for formulation A and to - 40°C for

**Table II.** Primary drying conditions for formulations A and B

Formulation	Experiment	Ramp rate from freezing (°C/min)	Shelf temperature (°C)	Chamber pressure (mTorr)	Duration of cycle* (h)
A	#0	0.5	- 30.0	50	66.0
A	#1	0.5	- 30.0	50	74.0
A	#2	0.5	- 25.0	50	57.4
A	#3	0.5	- 20.0	50	57.3
B	#0	1.4	- 35.0	50	155.3 <sup>†</sup>
B	#1	2.3	+ 0.0	150	39.9
B	#2	0.5	- 13.0	65	73.0
B	#3	0.5	- 12.0	65	100.0
B	#4	0.5	- 21.0	65	120.0

\*Duration of cycle is the time at which the shelf temperature and chamber pressure were maintained, not the time required to complete primary drying

†Did not complete primary during, no secondary drying

formulation B and held for 90 min to fully freeze the product. The ultimate freezing temperature was chosen to be sufficiently below thermal events for each formulation. Thermal data for Formulation A indicated a collapse temperature of  $-39^{\circ}\text{C}$  determined by freeze-drying microscopy (Lyostat, Linkam Scientific, Tadworth, UK). Formulation B exhibited a collapse temperature of  $-23^{\circ}\text{C}$  determined by freeze-drying microscopy and a  $T_g'$  of  $-26^{\circ}\text{C}$  determined by differential scanning calorimetry. Secondary drying conditions for both formulations A and B were chosen based on guidance from industry partners. Secondary drying for formulations A and B was conducted at  $25^{\circ}\text{C}$ , with a ramp rate of  $0.1^{\circ}\text{C}/\text{min}$  for formulation A and  $0.25^{\circ}\text{C}/\text{min}$  for formulation B.

### Determination of Vial Heat Transfer Coefficients from Sublimation Runs

Vial heat transfer coefficients for both 20R and 10R vials were determined by gravimetric based experiments. A full tray of vials (160 for 20R and 264 for 10R) was filled with deionized water (10 mL for 20R and 3 mL for 10R), and vials were semi-stoppered. Vials were loaded onto the middle shelf of a LyoStar 3 freeze-dryer using a “bottomless” tray. After cooling the shelf to  $-40^{\circ}\text{C}$  to freeze the water, the chamber pressure was set to 60, 100, or 150 mTorr and the shelf was set to  $-20$ ,  $0$ , or  $20^{\circ}\text{C}$ . Ice underwent sublimation at a fixed shelf temperature and pressure. The vacuum was released abruptly to end sublimation when  $\sim 1/3$  of the ice was removed as reported by the batch average TDLAS sensor, and the vials were brought to room temperature prior to weighing. Select vials were outfitted with 36-gauge thermocouple probes (Omega, Norwalk, CT) inserted through the rubber stopper and placed at the bottom center of the vial. Vials were selected to sample three vial location classes - center, inner-edge and outer-edge. The  $K_v$  values determined using this gravimetric method for each location class of vials was calculated from the average sublimation rate,  $\langle \dot{m}(t) \rangle$ , (weight of water removed/process time), times the heat of ice sublimation ( $670 \text{ cal/g}$ ),  $\Delta H_{\text{sub}}$ , the horizontal cross-sectional area of the vial  $A_v$ , ( $6.93 \text{ cm}^2$  for 20R and  $4.52 \text{ cm}^2$  for 10R), the shelf temperature,  $T_s$ , and the average product temperature,  $\langle T_b(t) \rangle$ , shown in Eq. 3.

$$K_v = \frac{\langle \dot{m}(t) \rangle \cdot \Delta H_{\text{sub}}}{A_v \cdot (T_s - \langle T_b(t) \rangle)} \quad (3)$$

This method for gravimetric determination of  $K_v$  is a simplified version of the method described by Pikal et al. (35).

Slight variations in number and placement of thermocouple probes, number of vials weighed, and methods to determine  $K_v$  for each vial location class were based on differences in protocols used by the two research groups performing the determinations. For both methods, thermocouples were placed in 4–5 outer-edge vials, 3 inner-edge vials, and 3–6 center vials and positioned at the bottom center of each vial. The water removed from each vial class divided by the sublimation time was taken as the average sublimation rate,  $\langle \dot{m}(t) \rangle$ . The thermocouple temperatures, sampled each

minute during sublimation, were averaged over the sublimation time,  $\langle T_b(t) \rangle$ , for each weighed vial. Individual vial heat transfer coefficients were determined at three chamber pressures and vials for each location class were averaged to determine  $K_v$  for center, inner-edge and outer-edge vials. Differences in the methods are as follows. *Method 1* was used for 10R vials, whereas *method 2* was used for 20R vials. In method 1, the vials outfitted with thermocouples were weighed before and after sublimation to determine the mass of water removed, whereas in method 2, all vials were individually weighed. In method 1, the beginning of sublimation was defined as when the isolation valve was opened following the extra freeze and pressure stabilization steps included in the freeze-dryer process recipe; the lyophilizer shelf temperature was raised from the  $-40^{\circ}\text{C}$  freezing temperature to the drying shelf setpoint temperature as fast as the lyophilizer could achieve (input ramp time was 0 min, actual ramp time was 12–13 min). In contrast, in method 2, the start of sublimation was defined as when the shelf temperature reached its set point; at this point, no more than 2% of the water had been removed from the vials. In method 1, the average  $T_s$  was calculated from the shelf heat transfer fluid inlet temperature measured by a resistance temperature detector (Omega, Norwalk, CT), whereas in method 2, the shelf temperature set point was used. The minor differences did not affect the values of  $K_v$  significantly but were described here to point out the level of detail that must be included in measurement protocols to obtain repeatability between research groups.

### Determination of Batch-Average Product Resistance Parameters

Product resistance as a function of dry layer thickness was determined for each formulation. A full tray of 10R vials was filled with a volume of 3 mL and 5.2 mL for formulations A and B, respectively. The formulations were dried under conservative shelf temperature / pressure conditions to avoid product collapse. Select vials were outfitted with 36-gauge thermocouple probes (Omega (Norwalk, CT)) inserted through the rubber stopper and placed at the bottom center of the vial. Thermocouples were placed in five outer-edge vials, three inner-edge vials and six center vials in the same configuration used during the  $K_v$  experiments for these vials. Product temperature at the sublimation interface was determined using Eq. 4:

$$T_p(t) = T_b(t) - \frac{\Delta H_s \cdot \dot{m}(t) \cdot L_{\text{ice}}(t)}{A_p \cdot K_{\text{ice}}} \quad (4)$$

where  $L_{\text{ice}}(t)$  is the thickness of ice in the vial,  $A_p$  is the area of the product, and  $K_{\text{ice}}$  is the thermal conductivity of ice ( $20.52 \text{ cal/h/cm/K}$ ) (36).  $T_b$  was measured using thermocouple probes, and  $\dot{m}(t)$  was continuously measured throughout the experiments using the batch average TDLAS sensor. All data were measured at 1-min intervals.  $L_{\text{ice}}$  was determined using Eq. 5:

$$L_{\text{ice}}(t) = \frac{m_o - m(t)}{\rho_{\text{ice}} \cdot A_p \cdot v_{\text{ice}}} \quad (5)$$

where  $m_o$  is the initial mass of water,  $m(t)$  is the mass of water removed at time  $t$  determined by integrating the TDLAS water vapor mass flow rate divided by the number of vials in the batch,  $\rho_{ice}$  is the density of ice (0.918 g/cm<sup>3</sup>), and  $v_{ice}$  is the volume fraction of ice (estimated at 0.97 for both formulations). Product and stopper resistance ( $R_{ps}$ ) was determined throughout the freeze-drying cycle using Eq. 6:

$$R_{ps}(t) = \frac{A_p \cdot (P_{ice}(t) - P_c)}{\dot{m}(t)} \quad (6)$$

where  $P_{ice}(t)$  is the vapor pressure of ice (37) determined from the product temperature at the sublimation interface (Eq. 7),  $T_p(t)$  (from Eq. 4) is the product temperature, and  $P_c$  is the chamber pressure measured using a capacitance manometer (MKS Instruments, Andover, MA).

$$P_{ice}(t) = 2.968 \times 10^{10} \cdot e^{-6144.96/T_p(t)} \quad (7)$$

The maximum dry layer thickness,  $L_{max}$ , of each formulation was calculated using Eq. 8, and the dry layer thickness as a function of time,  $L_{dry}(t)$ , was calculated using Eq. 9.

$$L_{max} = \frac{m_o / \rho_{ice}}{v_{ice} \cdot A_p} \quad (8)$$

$$L_{dry}(t) = L_{max} - L_{ice}(t) \quad (9)$$

Equation 10 was fit to  $R_{ps}(t)$  versus  $L_{dry}(t)$  to determine the product resistance parameters  $R_0$ ,  $A_1$ , and  $A_2$  using least squares regression.

$$R_{ps}(t) = R_0 + \frac{A_1 \cdot L_{dry}(t)}{A_2 + L_{dry}(t)} \quad (10)$$

### Determination of Equipment Capability Limits

Equipment capability limits were determined for the LyoStar 3 by performing ice slab sublimation tests under choked flow conditions. Ice slabs were formed on each shelf by lining a bottomless tray with a plastic sheet and filling with deionized water to a fill depth of approximately 2 cm. After cooling the shelf to  $-40^\circ\text{C}$  to freeze the water, the chamber pressure was set to 10 mTorr and the shelf was set to  $-40^\circ\text{C}$ . A chamber pressure set point of 10 mTorr was used to prevent the freeze dryer from bleeding nitrogen into the chamber, assuring only water vapor mass flow. Based on prior experience, it was known that the freeze-dryer could not achieve the low-pressure setpoint even at a shelf temperature of  $-40^\circ\text{C}$ , thus assuring an overload condition from the start of the experiment. The shelf temperature was raised in 10–20°C intervals up to  $60^\circ\text{C}$ , and sublimation was carried out at each shelf temperature for 45 to 60 min to allow for the establishment of steady-state operation. At each shelf temperature, the chamber pressure stabilized at the minimum controllable pressure. The pressure at the end of the steady state, defined as the average during the last 10 min at each

shelf temperature, was correlated with the water vapor mass flow determined by TDLAS at the same time interval to determine the equipment capability curve, shown as the pink line in the Primary Drying Process Design Space plot within Fig. 3.

### Location-Dependent $K_v$ and $R_p$ During Product Drying from Thermocouple-Reported Product Temperatures ( $T_p$ )

Location-dependent  $K_v$  and  $R_p$  values were determined for a subset of the model predictive verification drug substance lyophilization experiments. Thermocouple placements were identical to those used to determine  $K_v$  for 10R vials. For each vial outfitted with a thermocouple,  $K_v$  was calculated from the average sublimation rate,  $\langle \dot{m}(t) \rangle$ , using method 2 and average product temperature,  $\langle T_p(t) \rangle$ , using Eq. 3. The sublimation time was defined by subtracting the time at which sublimation started (marked by when the target shelf temperature for primary drying was reached) from the end of sublimation (marked by the rapid rise in the thermocouple temperature that indicates loss of contact with ice). The average sublimation rate,  $\langle \dot{m}(t) \rangle$ , was calculated using the initial mass of water in the vial,  $m_o$ , (not accounting for the negligible quantity of water associated with the amorphous phase) divided by the sublimation time.

The value of  $K_v$  for each vial was used along with the product temperature at each time point,  $T_p(t_i)$ , to calculate the product resistance  $R_p(t_i)$  for that vial at that time point using the following procedure. The sublimation rate at each time point was determined from Eq. 11.

$$\dot{m}(t_i) = \frac{K_v \cdot A_v \cdot (T_s - T_p(t_i))}{\Delta H_{sub}} \quad (11)$$

Taking the start of sublimation as  $t = 0$ , for all time points where  $t > 0$ , the average sublimation rate over each time interval,  $\Delta t_i = t_i - t_{i-1}$  equaled  $\frac{\dot{m}(t_i) + \dot{m}(t_{i-1})}{2}$ . The cumulative mass of ice removed,  $m(t_i)$  at the end of each time interval,  $t_i$ , equaled  $\frac{\sum_1^i \Delta t_i \dot{m}(t_i) + m(t_{i-1})}{2}$ . The dry layer thickness at the end of each interval,  $L_{dry}(t_i)$ , equaled the maximum dry layer thickness ( $L_{max}$ ) multiplied by the fraction of water removed up to the end of that interval,  $\frac{m(t_i)}{m_o}$ . The initial mass of water,  $m_o$ , was estimated to be 2.88 g in Formulation A and 4.75 g in Formulation B. The temperature of the sublimation interface,  $T_{p,i}$  was defined by Eq. 12, which is the single-vial version of Eq. 4

$$T_{p,i} = T_b(t_i) - \frac{\dot{m}(t_i) + \dot{m}(t_{i-1})}{2} \cdot \frac{\Delta H_{sub} \cdot L_{ice}(t_i)}{A_v \cdot K_{ice}} \quad (12)$$

The vapor pressure of water at the sublimation interface,  $P_{ice}(t_i)$ , was calculated from the temperature at the sublimation interface,  $T_{p,i}$  (Eq. 7). The total resistance to water vapor leaving the vial,  $R_{ps,i}$  (including both product and stopper resistance) for each interval,  $\Delta t_i$ , equaled  $\frac{A_p \cdot (P_{ice}(t_i) - P_c)}{\dot{m}(t_i)}$ , which



is the single vial version of Eq. 6. Thus, at each time point during primary drying, we calculated  $L_{dry}(t_i)$  and  $R_{ps, i}$  for each vial containing a thermocouple. Measuring  $R_p$  in each vial provides the data to determine  $R_p$  heterogeneity across the batch. However,  $R_p$  calculations using this method rely on accurate determination of primary drying times from thermocouple “breaks.” This is susceptible to errors due to the incorrect selection (should be thin gauge) and placement (should be at the bottom center of the vial) of thermocouple probes. To reduce errors, 36-gauge bare lead thermocouples were used, and probe placement was checked after the freeze-drying cycle. Although not used during the current model predictions, future versions of the software model will include the use of this  $R_p$  heterogeneity data. In addition to the current method of calculating vial specific values of  $R_p$ , a single vial tunable diode laser absorption spectroscopy-based mass flow measurement system is under development that should enable the determination of location dependent  $R_p$  values.

## RESULTS AND DISCUSSION

### Model Inputs: Vial Heat Transfer Coefficient

Vial heat transfer coefficients for three vial location classes—center, inner-edge, and outer-edge—were determined experimentally. The vial heat transfer coefficients,  $K_v$ , for all vials over all shelf temperatures showed the expected increase in  $K_v$  with chamber pressure (Table I). Of particular interest to modeling batch heterogeneity is the  $\% \Delta K_{v, edge}$ , which is the difference in the value of the vial heat transfer coefficient for edge vials,  $K_{v, outer edge}$ , over that for the center vials,  $K_{v, center}$ , expressed as a % of  $K_{v, center}$ . The smaller 10R vials had a marginally larger  $\% \Delta K_{v, edge}$  compared to the 20R vials at the same shelf temperature ( $-20^\circ\text{C}$ ).

At higher shelf temperatures, the  $\% \Delta K_{v, edge}$  was lower ( $\sim 23\%$  at a shelf temperature of  $0^\circ\text{C}$  and  $+20^\circ\text{C}$ ) and was less dependent on chamber pressure in the same range. This is consistent with previous theoretical finding that  $\% \Delta K_{v, edge}$  increases as  $T_s - T_b$  decreases (26). At a shelf temperature of  $-20^\circ\text{C}$ , the values of  $T_s - T_b$  during gravimetric sublimation experiments to determine  $K_v$  were 20, 17, and  $14^\circ\text{C}$  at

chamber pressures of 60, 100, and 150 mTorr, respectively. At higher shelf temperatures,  $T_s - T_b$  values were much higher,  $\sim 35^\circ\text{C}$  and  $50^\circ\text{C}$  at  $0^\circ\text{C}$  and  $+20^\circ\text{C}$ , respectively, consistent with the lower values of  $\% \Delta K_{v, edge}$ .

Perhaps more notable is the increase in center-vial  $K_v$  with shelf temperature. The value of  $K_v$  has been generally considered to be relatively independent of shelf temperature. While this is true in the usual low range of shelf temperatures ( $-25$  to  $-15^\circ\text{C}$ ),  $K_v$  is higher at the elevated shelf temperatures often used for protein formulations. Thus, additional information on heat transfer at elevated shelf temperatures will be useful. In this version of the software, the pressure-dependent but shelf temperature-independent  $K_v$  values for the 10R vials were input into the software (lower left table in Fig. 2). At intermediate pressures, the  $K_v$  is interpolated from given data. At higher ( $> 150$  mTorr) and lower ( $< 60$  mTorr) pressures, the  $K_v$  is extrapolated from the curve fit, but this approach carries a risk of inaccurate values of  $K_v$  due to extrapolation beyond the knowledge space.

$K_v$  values determined from thermocouple data collected during lyophilization of product in 10R vials (experimental data in Table III) were compared with  $K_v$  values at the experimental chamber pressure (model data in Table III) determined from interpolating/extrapolating data from water sublimation runs (Table I). Experimental  $K_v$  values were on average within 3% of interpolated/extrapolated  $K_v$  values used in the model for formulation A, experiment #1 and formulation B, experiment #3 (Table III), which both used low shelf temperatures ( $-30^\circ\text{C} < T_s < -21^\circ\text{C}$ ) during primary drying. The highest difference was  $\sim 12$ – $19\%$  during the most aggressive drying cycle ( $T_{shelf} = 0^\circ\text{C}$ ) of formulation B, where higher  $K_v$  values are expected due to the higher shelf temperature as shown in Table I. In addition, for this case the  $\% \Delta K_{v, edge}$  determined from thermocouples during lyophilization of product (Table III, Exp) was only 3% compared to 44% as determined from the ice sublimation (Table III, Model). Future refinement of the model to better account for  $K_v$  heterogeneity as a function of shelf temperature will improve the agreement.

### Model Inputs: Product Resistance

For each formulation, batch-average product resistance was determined using TDLAS water vapor mass flow rate measurements as a function of dry layer thickness during a conservative experiment designed to avoid any frozen drug formulation structural changes (viscous flow) that would affect the resistance of the product. Primary drying conditions (for experiment #0 in Table II) maintained the frozen drug product below estimated  $T_c$  (formulation A) and  $T_g'$  (formulation B) values for each formulation. In the case of formulation A, the product resistance determined *a priori* from the conservative cycle, experiment #0, represented the product behavior well even during the slightly more aggressive cycles, experiments #1–3, (Fig. 4A), with  $R_p$  increasing linearly with  $L_{dry}$ . In addition, the resistance was relatively low,  $\sim 3.0 \text{ cm}^2 \cdot \text{Torr} \cdot \text{h/g}$  at  $2/3L_{max}$ . Formulation B, on the other hand, had a higher resistance ( $\sim 13.0 \text{ cm}^2 \cdot \text{Torr} \cdot \text{h/g}$  at  $2/3L_{max}$ ) and exhibited a cycle-dependent  $R_p$  (Fig. 4B). Additionally, the product resistance measured using a conservative cycle, experiment #0, *a priori* for model input was much

**Table III.** Accuracy of vial heat transfer coefficient model inputs compared to experimentally measured values  $\times 10^4 \text{ cal/cm}^2/\text{s/K}$

Experiment	Vial class	Model	Exp.	%Difference
Formulation A	Center	2.14	2.15	-0.5%
Experiment #1 $T_s = 30.0^\circ\text{C}$	Inner edge	2.72	2.68	1.5%
	Outer edge	3.30	3.48	-5.2%
Formulation B	Center	3.21	3.96	-18.9%
Experiment #1 $T_s = 0.0^\circ\text{C}$	Inner edge	3.92	4.46	-12.1%
	Outer edge	4.61	4.07	13.3%
Formulation B	Center	2.32	2.49	-6.8%
Experiment #2 $T_s = -13.0^\circ\text{C}$	Inner edge	2.87	3.05	-5.9%
	Outer edge	3.45	3.26	5.8%
Formulation B	Center	2.32	2.22	4.5%
Experiment #3 $T_s = -21^\circ\text{C}$	Inner edge	2.87	2.89	-0.7%
	Outer edge	3.45	3.21	7.5%

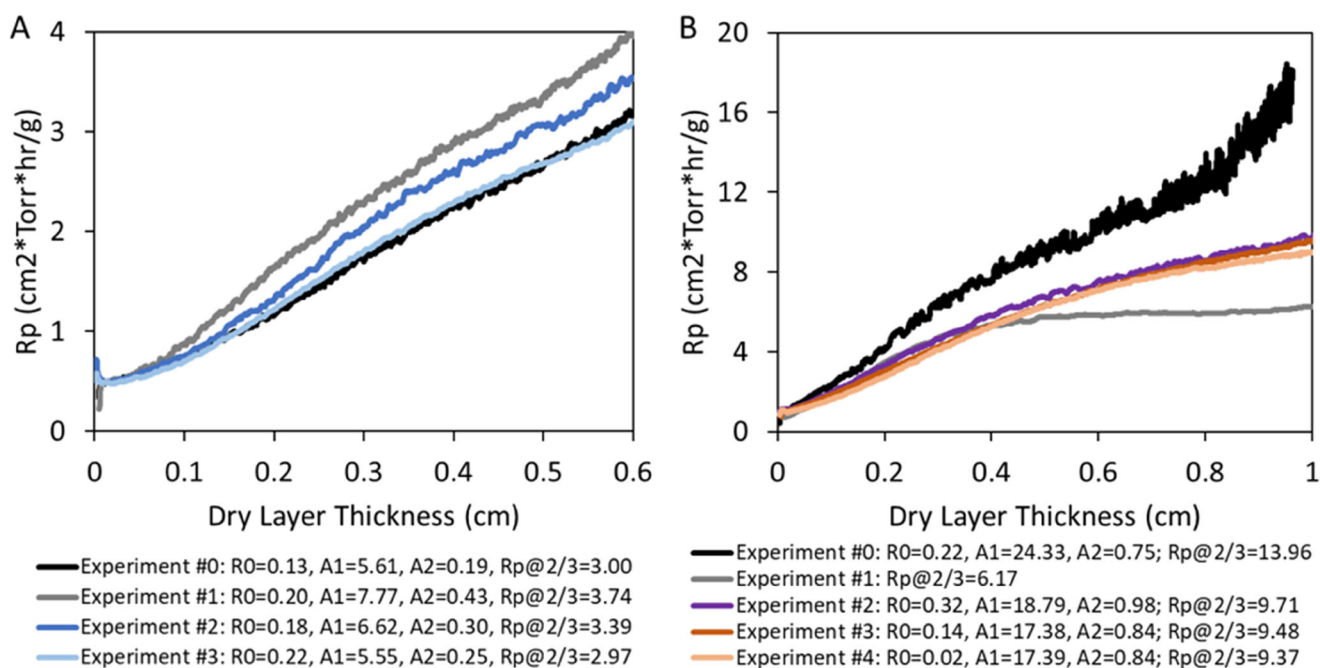


**Fig. 4.** Product resistance as a function of dry layer thickness for the first 2/3 of primary drying for **A** formulation A and **B** formulation B for all experiments. Drying conditions for each experiment are listed in Table II

higher than the product resistance measured during freeze-drying of the product using more aggressive cycles, experiments #1–4. Equation 10 was fit to the product resistance to determine the  $R_p$  parameters  $R_0$ ,  $A_1$ , and  $A_2$  within the modeling software using least squares regression, except for formulation B #1, which was not adequately fit by Eq. 10 (Supplemental Fig. 1). The mean squared errors of the fit to the  $R_p$  data (calculated using the batch average TDLAS mass flow rate measurements) for formulations A and B were 0.0026 and 0.0907, respectively, for the experiment #0 cycles.

### Determining Model-Derived Primary Drying Process Conditions

Primary drying process conditions for each product were determined by first entering vial, product and lyophilizer parameters into the *Design Space Inputs* screen (Fig. 2) of the software tool. Model parameters including product resistance ( $R_0$ ,  $A_1$ , and  $A_2$  from experiment #0 for each formulation, in this case), *Vial Heat Transfer Coefficients versus Pressure* (for 10R vials from Table I in this case) and *Equipment Capability Limits* (shown in Fig. 2) were also entered. Additional inputs included the *Solute Concentration*, *Fill Volume*, *Vial Type*, and *Number of Vials* filled with product formulation. When known, experimentally derived %RSD values can be input for each parameter, including the  $R_p$  parameters  $R_0$  and  $A_1$  (Eq. 10). However, for the present study, default values available in the software were selected from a drop-down menu (25). An initial estimate of process conditions, including *Shelf Setpoint Temperature*, *Chamber Pressure* and *Primary Drying Cycle Time* were input. If the shelf temperature standard deviation is unknown, the software can calculate a value based on *Shelf Temperature Measurements* experimental data input into the lower righthand table (Fig. 2). An initial *Shelf Setpoint Temperature* and *Chamber Pressure* can also be calculated by the software using a previously published algorithm (9). Finally, the *Vials Allowed to*

*Collapse* was specified to enable the calculation of the *Average Edge Vial Temperature at the # of Vials Allowed to Collapse* in the *Primary Drying Process Design Space* plot in the *Calculation and Results* user interface. A typical input is one (1) vial allowed to collapse.

After inputting the required parameters, the model performed calculations to predict the product temperature (by location), drying time, percentage of collapsed vials, percentage of vials that did not complete drying and the primary drying process design space in the *Calculations and Results* user interface. Following review of the results based on the initial set of process conditions, an iterative process was used to improve the process efficiency with the goal of shorter drying times while maintaining product quality: product temperature in all vial locations below the collapse temperature, low percentage of collapsed vials and vials not dry. The iterative process included review of:

- I.  $P_{ice}$  vs Drying Time: All calculated pressures above the chamber pressure to ensure a driving force for sublimation
- II. *Average Safety Margin*: Typically maintained between 2 and 4°C
- III.  $T_p$  vs Drying Time: Edge vials that typically possess the highest  $K_v$  value are maintained below the collapse temperature especially near the end of primary drying
- IV. % Vials Collapsed: Typically maintained between 0.5 and 0.0003% (6-sigma)
- V. % Vials Not Dry: Typically maintained between 0.5 and 0.0003% (6-sigma)
- VI. *Primary Drying Process Design Space*: Target operating conditions located below the apex crossing of the equipment capability curve and the average edge vial product temperature isotherm at the user-defined number of vials allowed to collapse

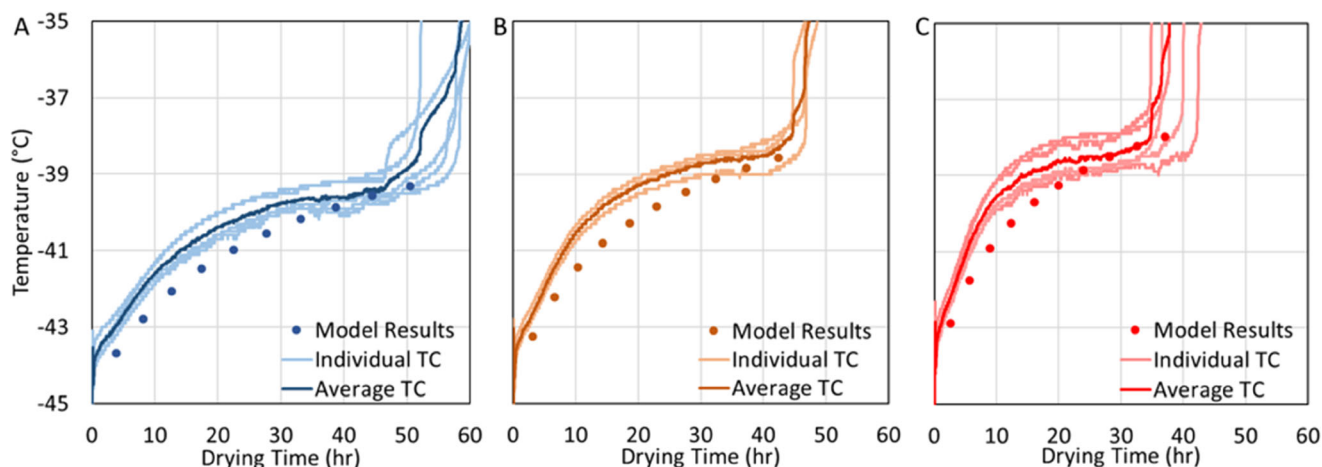


**Fig. 5.** Formulation A, experiment #1, comparison of model results of product temperature at the bottom center of the vial to product temperatures measured by thermocouple probes (TC) for **A** center ( $n = 6$ ), **B** inner edge ( $n = 3$ ), and **C** outer edge ( $n = 5$ ) vials. The data shows good agreement between model predictions and observed product temperatures as well as primary drying times

Changes were made to the *Shelf Setpoint Temperature* to maintain vials below the *Collapse Temperature*, adjust the *Average Safety Margin* and to adjust the *% of Vials Collapsed*. Adjustments were made to the *Primary Drying Cycle Time* to affect the *% Vials Not Dry*. The *Chamber Pressure* was adjusted to position the target operating conditions under the apex of the *Primary Drying Process Design Space*.

The process described above was performed for each experiment performed for formulations A and B. The *Shelf Setpoint Temperature* and *Chamber Pressure* input parameters were adjusted to challenge the predictive capability of the software model and to explore how changes to product resistance due to changing operating conditions (and product

temperature) affect the predictive capability of the primary drying model. These results are discussed below.

#### Model Accuracy: Product Temperature and Primary Drying Time

The primary drying conditions for formulation A, experiment #1 matched the conditions of the cycle to determine product resistance experiment #0, with subsequent experiments increasing the shelf temperature in 5°C increments with the chamber pressure held constant. The model predicted an increasing percentage of collapse with increasing

**Table IV.** Model accuracy in predicting primary drying time and product temperature prediction

Experiment	Vial class	Primary drying time			Product temperature		
		Model mean (h)	Experimental mean $\pm$ std dev (h)	% Difference	Model mean (°C)	Experimental mean $\pm$ std dev (°C)	° C Difference
Formulation A #1	Center	50.5	53.6 $\pm$ 3.3 ( $n=6$ )	6.1	-41	-40.4 $\pm$ 0.2 ( $n=6$ )	-0.6
	Inner edge	42.4	47.3 $\pm$ 3.8 ( $n=3$ )	11.6	-40.4	-39.4 $\pm$ 0.6 ( $n=3$ )	-0.1
	Outer edge	37.1	43.0 $\pm$ 13.8 ( $n=5$ )	15.9	-39.8	-39.2 $\pm$ 0.4 ( $n=5$ )	-0.6
Formulation B #1	Center	29.7	21.1 $\pm$ 1.6 ( $n=6$ )	28.6	-21.6	-24.4 $\pm$ 0.9 ( $n=6$ )	2.8
	Inner edge	25.8	19.0 $\pm$ 1.1 ( $n=3$ )	26.4	-20.4	-23.6 $\pm$ 0.6 ( $n=3$ )	3.2
	Outer edge	23.2	20.3 $\pm$ 2.2 ( $n=5$ )	12.5	-19.4	-24.5 $\pm$ 0.8 ( $n=5$ )	5.1
Formulation B #2	Center	55.9	45.7 $\pm$ 3.2 ( $n=6$ )	18.2	-28.8	-30.6 $\pm$ 0.8 ( $n=6$ )	1.8
	Inner edge	48.8	40.3 $\pm$ 9.5 ( $n=3$ )	17.4	-27.6	-30.1 $\pm$ 0.8 ( $n=3$ )	2.5
	Outer edge	43.6	37.8 $\pm$ 3.4 ( $n=5$ )	13.3	-26.7	-29.6 $\pm$ 2.0 ( $n=5$ )	2.9
Formulation B #2 (in-process $R_p$ )	Center	5.4	-45.7 $\pm$ 3.2 ( $n=6$ )	9.3	-30.4	-30.6 $\pm$ 0.8 ( $n=6$ )	0.2
	Inner edge	43.7	-40.3 $\pm$ 9.5 ( $n=3$ )	7.8	-29.3	-30.1 $\pm$ 0.8 ( $n=3$ )	0.8
	Outer edge	38.8	-37.8 $\pm$ 3.4 ( $n=5$ )	2.6	-28.4	-29.6 $\pm$ 2.0 ( $n=5$ )	1.2
Formulation B #3	Center	82.7	72.0 $\pm$ 7.3 ( $n=6$ )	12.9	-31.7	-33.7 $\pm$ 0.4 ( $n=6$ )	2.0
	Inner edge	73.1	-59.8 $\pm$ 2.8 ( $n=3$ )	18.2	-30.8	-32.6 $\pm$ 0.4 ( $n=3$ )	1.8
	Outer edge	66.2	-56.7 $\pm$ 5.7 ( $n=5$ )	14.4	-30.1	-32.1 $\pm$ 0.5 ( $n=5$ )	2.0
Formulation B #3 (in-process $R_p$ )	Center	72.1	-72.0 $\pm$ 7.3 ( $n=6$ )	0.1	-33.2	-33.7 $\pm$ 0.4 ( $n=6$ )	0.5
	Inner edge	63.1	-59.8 $\pm$ 2.8 ( $n=3$ )	5.2	-32.3	-32.6 $\pm$ 0.4 ( $n=3$ )	0.3
	Outer edge	56.5	-56.7 $\pm$ 5.7 ( $n=5$ )	0.4	-31.6	-32.1 $\pm$ 0.5 ( $n=5$ )	0.5

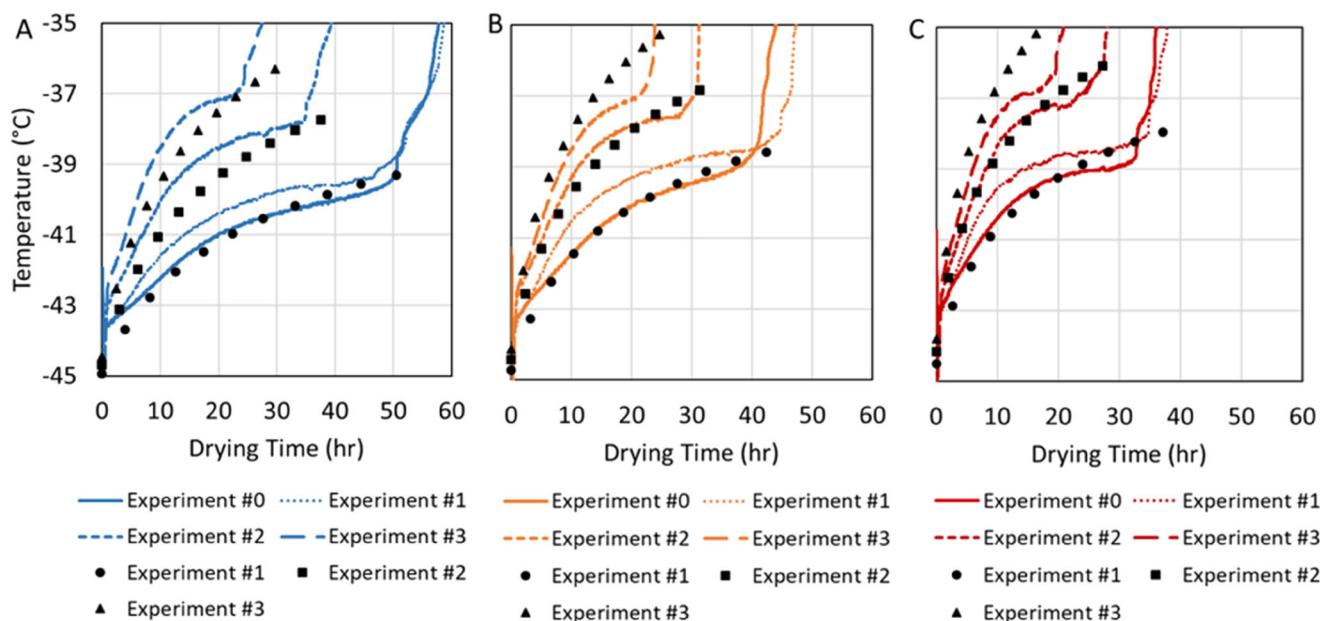


**Fig. 6.** Formulation A, experiments #0–#3, average product temperatures measured by thermocouple probes (solid lines) and model results for product temperature at the bottom center of the vial based on  $R_p$  from experiment #0 (markers) for **A** center ( $n = 6$ ), **B** inner edge ( $n = 3$ ), and **C** outer edge ( $n = 5$ ) vials. The data shows variance in product temperature with primary drying conditions (shelf temperature and chamber pressure)

average product temperature due to the higher shelf temperatures. Using the collapse temperature estimated from freeze drying microscopy,  $-39.0^{\circ}\text{C}$ , the model predicted 39% of vials collapsed in experiment #1, 99.8% in experiment #2, and 100% in experiment #3. On 100% visual assessment of dried cakes from all cycles, there was no macrocollapse, only modest shrinkage of the cake. For formulation B, conditions for experiment #1 were chosen to be highly aggressive with 97% collapse predicted, whereas conditions for experiments #2 and #3 were predicted to maintain maximum outer edge vial temperatures below the measured  $T_c$  (with a  $1.5^{\circ}\text{C}$  safety

margin) and  $T_g'$  ( $2.2^{\circ}\text{C}$  safety margin) respectively. Experiment #4 was a repeat of experiment #3. Again, 100% visual assessment of vials showed no macrocollapse, only increasing cake shrinkage for the more aggressive cycles. The %collapse results, while not in agreement with model predictions, are consistent with reported reduced collapse of protein formulations in vials than in the thin film format used in freeze drying microscopy (14). These results highlight the need to better define the collapse temperature used to design a cycle for a protein formulation relative to the collapse temperature determined by freeze-drying microscopy or  $T_g'$  (38).

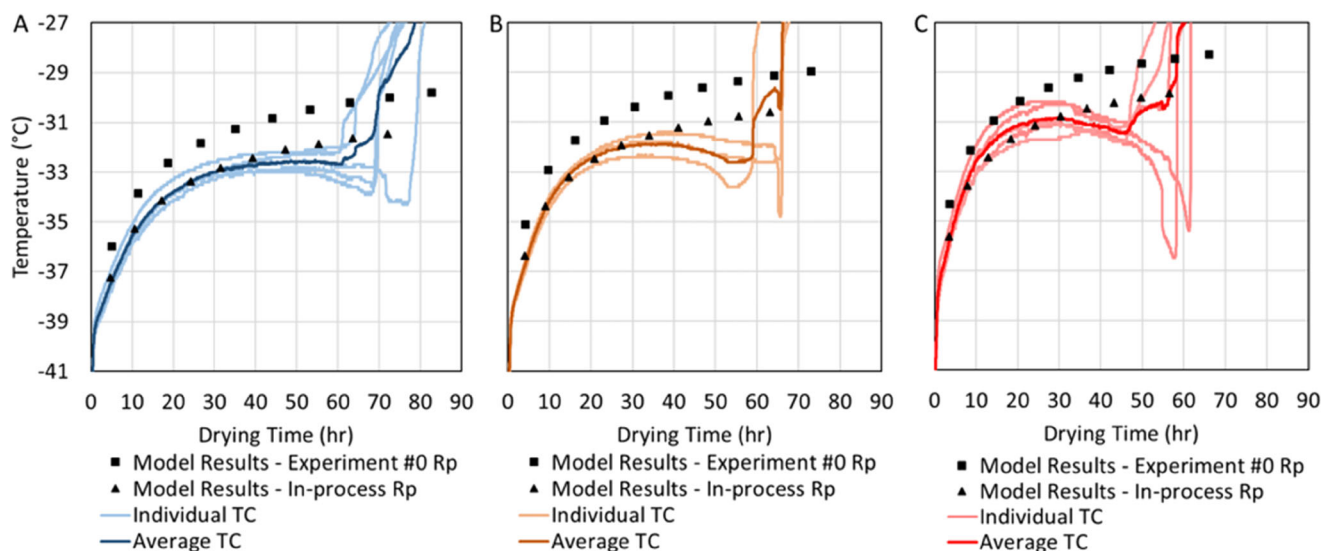


**Fig. 7.** Formulation B, experiment #3, comparison of model results of product temperature at the bottom center of the vial based on  $R_p$  calculated from experiment #0 or an in-process determined  $R_p$  and product temperatures measured by thermocouple probes for **A** center ( $n = 6$ ), **B** inner edge ( $n = 3$ ), and **C** outer edge ( $n = 5$ ) vials. Model accuracy is significantly improved using in-process determined  $R_p$  parameters due to changes in product resistance between cycles

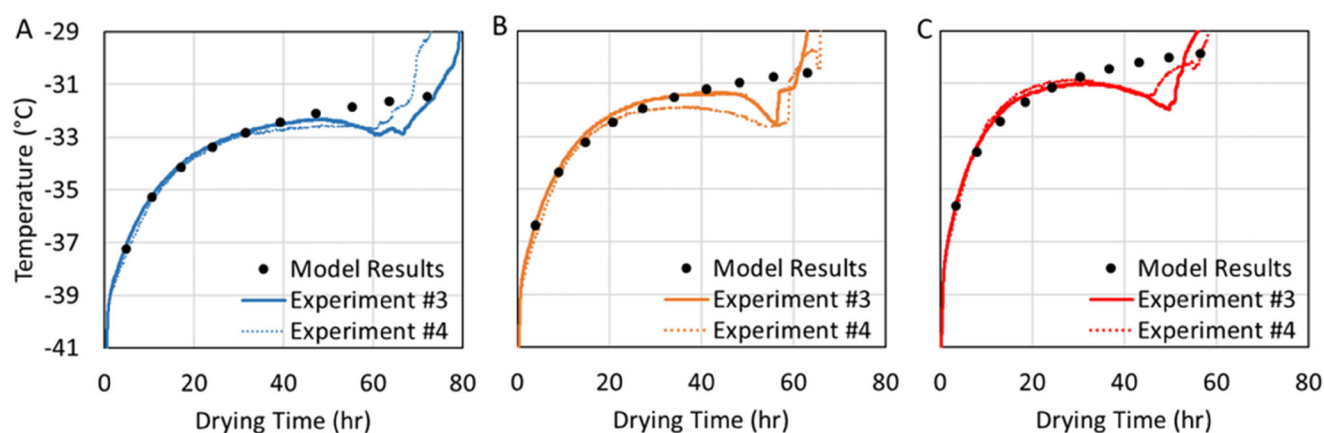


**Fig. 8.** Formulation B, comparison of model results of product temperature at the bottom center of the vial using in-process  $R_p$  from experiment #3 and average product temperatures measured by thermocouple probes for **A** center ( $n = 6$ ), **B** inner edge ( $n = 3$ ), and **C** outer edge ( $n = 5$ ) vials for experiments #3 and #4. The data shows good agreement between model predictions and observed product temperatures and reproducibility between cycles with the same primary drying conditions

The model-predicted location-based average product temperature was compared to product temperatures measured using thermocouple probes positioned touching the bottom center of selected center, inner-edge and outer-edge vials during freeze-drying experiments. Product probe placement was identical to the placement used during 10R vial sublimation runs to determine  $K_v$ , and conservative Experiments (#0) to determine  $R_p$ . The model predictions for Formulation A (using  $R_p$  from Experiment #0, filled circles in Fig. 5) and experimental average product temperature profiles (dark lines in Fig. 5) during primary drying Experiment #1, for each vial location class, agree within  $\sim 1^\circ\text{C}$  with experimentally determined product temperatures. The experimental measurements were slightly higher than predicted by the model, most likely due to the higher experimental product resistance (Fig. 4A). However, late in primary drying, where the product temperature is higher and the product more vulnerable to collapse, the agreement was improved. The average difference between the model predicted  $T_b$  and the experimentally measured  $T_b$  was  $-0.6^\circ\text{C}$  for center vials,  $-1.0^\circ\text{C}$  for inner edge vials, and  $-0.6^\circ\text{C}$  for outer edge vials (Table IV).

The heterogeneity in experimental product temperatures is evident from the individual thermocouple traces (Fig. 5,

lighter colored lines). Even within a vial location class, there is some variation in  $T_b$  due to heterogeneity in  $K_v$  and  $R_p$ . Additional heterogeneity in product temperature can be attributed to measurement variations due to thermocouple placement. The product temperature profiles of Formulation A during primary drying at increasing shelf temperature agree well with the model predictions (Fig. 6). The average absolute difference between the model predicted  $T_b$  and the experimentally measured  $T_b$  was less than  $1^\circ\text{C}$  for all vial location classes for all experiments (data not shown), based on product temperature data before completion of primary drying.

While the product temperatures predicted by the model for formulation A matched the experimental results reasonably well, the predictive capability of the model was challenged by formulation B. Average product temperatures that were predicted by the model using the  $R_p$  (Fig. 4B) from the conservative (#0) cycle were higher by as much as  $2^\circ\text{C}$  (Fig. 7) than average experimental product temperatures (dark lines in Fig. 7) in Experiment #3, which used more aggressive drying conditions. Vial heat transfer coefficients calculated from thermocouple-reported product temperatures (method 2) showed that the model inputs were within 5% for center and inner edge vials, while outer edge vials had a 7% difference between experimental values and model inputs

**Table V.** Product resistance at 2/3 of  $L_{\max}$  for each vial class

	$R_p$ at 2/3 of drying ( $\text{cm}^2\cdot\text{h}\cdot\text{Torr/g}$ )		
	Center ( $n=5$ )	Inner edge ( $n=3$ )	Outer edge ( $n=5$ )
Formulation A Experiment #1	$3.95 \pm 1.25$	$4.71 \pm 0.37$	$3.83 \pm 0.37$
Formulation B Experiment #1	$6.68 \pm 0.87$	$6.87 \pm 1.33$	$5.84 \pm 1.66$
Formulation B Experiment #2	$10.22 \pm 0.62$	$9.33 \pm 3.01$	$7.80 \pm 0.53$
Formulation B Experiment #3	$10.98 \pm 1.51$	$10.41 \pm 1.20$	$9.90 \pm 1.09$

(Table III). Modeling the cycle using in-process determined  $K_v$  values calculated from data collected during the product drying experiment did not fully resolve the product temperature inaccuracy (data not shown).

Product resistance was considered as another possible source of prediction inaccuracy. The  $R_p$  for cycle #0 was dramatically higher than the  $R_p$  for cycle #3 (Fig. 4B). There were substantial differences in  $R_p$  as a function of dry layer thickness for formulation B at different shelf temperature/pressure operating conditions. Product resistance was significantly lower for all four model verification product formulation experiments (#1–4) compared to the initial conservative product resistance experiment (#0). While all cakes were acceptable in appearance, with no apparent macrocollapse, the decrease in product resistance suggested microcollapse (changes in the cake micro-structure that reduced resistance to vapor flow out of the cake, without significant change in shape of the overall cake). For a more aggressive cycle, experiment #3 compared to experiment #0, average product temperatures for center vials were higher ( $-33.7 \pm 0.4^\circ\text{C}$ ) than those in cycle #0 ( $-40.4 \pm 0.2^\circ\text{C}$ ) with correspondingly higher temperatures for inner and outer edge vials (Table IV). While the  $T_{b,av}$ , center for experiment #3 was higher than experiment #0, it was lower than predicted by the model ( $-31.7^\circ\text{C}$ ) when using experiment #0  $R_p$  (Table IV). At the higher product temperatures, particularly those near and above  $T_g'$ , which was difficult to conclusively determine for this formulation, viscous flow is expected to be greater. Viscous flow collapses small pores that consolidate into larger pores, reducing the product resistance. At sufficiently high product temperatures, collapse of the entire structure, or macrocollapse, can yield an unacceptable product appearance.

When the model was used to predict the product temperatures using a batch average  $R_p$  derived from the same cycle (triangles in Fig. 7), agreement significantly improved. Average product temperatures were predicted to within  $0.5^\circ\text{C}$  for all vial location classes compared to  $2.0^\circ\text{C}$  with the inaccurate  $R_p$ . As a further test of the model, formulation B was dried (experiment #4) using identical cycle conditions to the previous experiment #3. Average product temperatures using the product resistance data from experiment #3 agreed well (Fig. 8) with the experimental product temperature for the repeat experiment (#4), except at the end of primary drying, where the time-dependent microcollapse became difficult to model with this version of the software. Similar results were obtained for experiment #2 for formulation B where product temperature accuracy is significantly improved using in-process  $R_p$  data for defining model inputs (Table IV). However, there is reduced model accuracy for inner and outer edge vials due to more appreciable product temperature drops (similarly to Fig. 7) late in primary drying. The equation traditionally used for  $R_p$  (Eq. 10) does not allow for modeling of product temperature decreases during the cycle.

The same method of using in-process  $R_p$  to model the cycle could not be applied to experiment #1 due to the magnitude of the reduction in  $R_p$  caused by microcollapse. As shown in Fig. 4B,  $R_p$  for experiment #1 plateaued at an  $L_{dry} > 0.4$  cm. The equation used to define  $R_p$  as a function of dry layer thickness (Eq. 10) could not be fit to this data;

therefore, the current model could not be used. An alternative data fitting method is being explored. In summary, when the degree of microcollapse increases with the product temperature as in formulation B (supplemental Fig. 2), the current model cannot account for lower product temperature during primary drying due to the reduced product resistance. Model accuracy is limited both late in the cycle and for edge vials where the effect of microcollapse is most evident. Future versions of the model software will include modified fitting solutions to “atypical”  $R_p$  curves that are not currently fit by the standard  $R_p$  fit equation, accommodating cycles designed to include microcollapse as a method of shortening cycle time while not compromising defined product quality attributes.

A more subtle difference in  $R_p$  was also identified, particularly for formulation B, in the more aggressive experiments (#1 and #2). During these aggressive cycles, the experimentally measured product temperatures were much lower than model predictions in the outer edge vials than the center vials (Table IV). The lower than model-predicted  $K_v$  in the edge vials (Table III) does not completely account for the lower than model-predicted product temperatures in the edge vials. Furthermore, the experimental drying times for vials with lower  $K_v$  values should be theoretically longer, but in the edge vials, the drying times are shorter than predicted by the model. This suggests greater microcollapse in the outer edge vials that reduces the  $R_p$  of the product. The  $R_p$  (at 2/3 through primary drying) of the cakes trended with decreasing average product temperature during primary drying (supplemental Fig. 2). For example, in center vials, the average product temperature during the three experiments (#1, #2, and #3) were  $-24.4$ ,  $-30.6$ , and  $-33.7^\circ\text{C}$ , and the corresponding  $R_p$  values were 6.7, 10.2, and 11.0 at 2/3 through primary drying (Table V). For the most conservative cycle (#3), the  $R_p$  for edge vials was lower by 10%. For the most aggressive cycle (#1), the  $R_p$  for edge vials was 13% lower. Capturing this type of cycle-dependent, location-dependent  $R_p$  heterogeneity will allow the model to more fully describe the heterogeneity across the batch.

The model was also evaluated for its ability to predict primary drying times. For formulation A, during experiment #1, the mean drying times predicted by the model agreed fairly well (6% lower than the experimental average) for center vials, with greater deviation for edge vials (12% and 16% lower than experimental averages for inner and outer edge vials, respectively) (Table IV). However, these were determined using relatively few thermocouples (3–6) at each location. Perhaps, the better comparison is that the model predictions of location-dependent mean drying times were within 1.4 standard deviations from the experimentally determined drying times (as determined by the thermocouple “break” or sudden rise in thermocouple temperature).

Formulation B required the use of in-process  $R_p$  values for the model to predict the location-dependent drying times. Using the  $R_p$  determined from Experiment #0, the average drying times predicted for Formulation B were as much as 13–29% higher than the experimentally determined averages (Table IV). However, when in-process  $R_p$  values that better characterized the internal cake structure were used in the model, the predictions were higher by only 0–9% or within 1.5 standard deviations of the experimentally determined mean times. Since only a few vials (14 of 264) can be outfitted

with thermocouples, based on these experiments, drying time can only be predicted to within 1–2 standard deviations. The full distribution of drying times (Fig. 3, upper right-hand plot) provides a better picture of the heterogeneity of drying across the batch (including that due to vial location, cake resistance, fill volume, and shelf temperature).

## CONCLUSIONS

A user-friendly software package was developed from two previously described models (25, 26) to provide a new tool for process development and scale-up. This publication focuses on use of the tool for process development. A future publication will focus on the process scale-up capability of the software. Two industry-supplied drug formulations were used to test the ability of the new tool to develop primary drying cycles and correctly predict product temperatures and drying times. Using experimentally derived inputs for all parameters, it was demonstrated that the software model was capable of accurately predicting the product temperature by vial location class, center, inner-edge and outer-edge, to within 1°C. Drying times were accurately predicted to within 10% for formulation A center vials and all formulation B vials using in-process  $R_p$  determinations.

This observation highlights a critical factor in the predictive accuracy of the software model, the product resistance to drying,  $R_p$  input. Experiments were performed over a range of shelf temperature and pressure conditions, some which included the product temperature exceeding the collapse,  $T_c$ , and glass transition temperatures,  $T_g'$ . This resulted in microcollapse of the product and dry layer thickness-dependent differences between  $R_p$  determined under conservative and more aggressive conditions. These conditions also resulted in corresponding reductions in product temperatures as a function of process time. When significant microcollapse occurred, the typical  $R_p$  equation was not always applicable to fitting  $R_p$  as a function of dry layer thickness and the  $R_p$  determined under conservative conditions was no longer accurate. An “in-process”  $R_p$  curve was required to accurately predict product temperatures and primary drying times.

New approaches for addressing this atypical  $R_p$  behavior, often observed in protein formulations, are planned for the next version of the model. In addition, both the  $T_c$  from freeze-drying microscopy and  $T_g'$  may not be appropriate “critical temperatures” to use in process design for protein formulations, since from an industry manufacturing perspective, microcollapse may be acceptable and in fact desirable. Using the standard “critical temperatures”, the model predicted a higher % of product collapse than was observed using 100% visual assessment, where only cake shrinkage was evident. Once the required cake appearance has been defined for the product, the product temperature limit or “critical temperature” that produces cakes with an acceptable appearance (38) is probably more appropriate to use in the model. The challenges associated with measuring and modeling  $R_p$  under conditions of product microcollapse highlight the need for new technology that can quantify microcollapse and a model that can predict microcollapse as a function of product temperature to support process development and scale-up for biopharmaceuticals.

In the future, an updated approach to model usage includes the need for the end-user to perform a parametric study of product resistance to drying as a function of product temperature if microcollapse is allowed to occur. This study will define the range of acceptable product temperatures that can be accurately predicted with unchanging  $R_p$  values determined prior to use of the model for the prediction of accurate product temperatures and drying times.

In the current study, the heterogeneity across the batch was captured in part by the location-dependent average product temperature profiles measured and predicted during primary drying. Model predictions of heterogeneity within each vial location class (center, inner-edge, outer-edge) is still to be evaluated by collection of additional product temperature profiles currently limited by the number of thermocouples. In addition to the well-known location-dependent  $K_v$  heterogeneity, initial evidence for location-dependent  $R_p$  heterogeneity was also identified. At elevated shelf temperatures, where the current model did not fully capture the location-dependent  $K_v$  heterogeneity, the lower true  $R_p$  in edge vials partially compensated for higher heat input, resulting in acceptable agreement of product temperatures during primary drying. In future efforts, full characterization of location- and shelf temperature-dependent  $K_v$  as well as location- and product temperature-dependent  $R_p$  will enhance the accuracy of the predictions by the model within the user-friendly software.

## SUPPLEMENTARY INFORMATION

The online version contains supplementary material available at <https://doi.org/10.1208/s12249-021-02134-3>.

## AUTHOR CONTRIBUTIONS

All authors contributed to the study conception and design. Material preparation, data collection, and analysis were performed by Robin Bogner, Emily Gong, William Kessler, and Arushi Manchanda. Michael Hinds developed the software. Jessie Zhao, Puneet Sharma, Akhilesh Bhambhani, and Justin Stanbro provided drug substance. The first draft of the manuscript was written by Robin Bogner, Emily Gong, and William Kessler, and all authors commented on previous versions of the manuscript. All authors read and approved the final manuscript.

## FUNDING

This work was performed under a Project Award Agreement from the National Institute for Innovation in Manufacturing Biopharmaceuticals (NIIMBL) and financial assistance award 70NANB17H002 from the US Department of Commerce, National Institute of Standards and Technology. Drug substance was provided at no cost by Genentech and Merck.

## DECLARATIONS

**Conflict of Interest** The authors declare no competing interests

## REFERENCES

- SEQENS. What is driving the growing demand for lyophilization? Available from: <https://cdmo.seqens.com/api-manufacturing/what-is-driving-the-growing-demand-for-lyophilization/>, [Accessed 24<sup>th</sup> April 2020].
- Chang BS, Reilly M, Chang H. Lyophilized biologics. In: Varshney D, Singh M, editors. *Lyophilized biologics and vaccines: modality-based approaches*. New York: Springer; 2015.
- Pikal MJ. Freeze drying. In: *Encyclopedia of pharmaceutical technology*, vol. 1299. N Y: Marcel Dekker; 2002. p. 1326.
- Mirasol F. Lyophilization presents complex challenges. *BioPharm Int*. 2020;33(1).
- Chang BS, Fischer N. Development of an efficient single-step freeze-drying cycle for protein formulations. *Pharm Res*. 1995;12(6):831–7.
- Mockus LN, Paul TW, Pease NA, Harper NJ, Basu PK, Oslos EA, Sacha GA, Kuu WY, Hardwick LM, Karty JJ, Pikal MJ, Hee E, Khan MA, Nail SL. Quality by design in formulation and process development for a freeze-dried, small molecule parenteral product: a case study. *Pharm Dev Technol*. 2011;16(6):549–76.
- Patel SM, Pikal MJ. Lyophilization process design space. *J Pharm Sci*. 2013;102(11):3883–7.
- Roy ML, Pikal MJ. Process control in freeze drying: determination of the end point of sublimation drying by an electronic moisture sensor. *J Parenter Sci Technol*. 1989;43:60–6.
- Tang X, Pikal MJ. Design of freeze-drying processes for pharmaceuticals: practical advice. *Pharm Res*. 2004;21(2):191–200.
- Schneid SC, Gieseler H, Kessler WJ, Luthra SA, Pikal MJ. Optimization of the secondary drying step in freeze drying using TDLAS technology. *PharmSciTech*. 2011;12(1):379–87.
- Rambhatla S, Tchessalov S, Pikal MJ. Heat and mass transfer scale-up issues during freeze-drying, III: control and characterization of dryer differences via operational qualification tests. *PharmSciTech*. 2006;7(2):E61–70.
- MacKenzie A. Collapse during freeze drying – qualitative and quantitative aspects. In: Goldblith S, Rey L, Rothmayr W, editors. *Freeze drying and advanced food technology*. London: Academic Press; 1975.
- Pikal MJ, Shah S. The collapse temperature in freeze-drying - dependence on measurement methodology and rate of water removal from the glassy phase. *Int J Pharm*. 1990;62(2–3):165–86.
- Greco K, Mujat M, Galbally-Kinney KL, Hammer DX, Ferguson RD, Iftimia N, Mulhall P, Sharma P, Kessler WJ, Pika MJ. Accurate prediction of collapse temperature using optical coherence tomography-based freeze-drying microscopy. *J Pharm Sci*. 2013;102(6):1773–85.
- Depaz RA, Pansare S, Patel SM. Freeze-drying above the glass transition temperature in amorphous protein formulations while maintaining product quality and improving process efficiency. *J Pharm Sci*. 2016;105(1):40–9.
- Johnson R, Lewis L. Freeze-drying protein formulations above their collapse temperatures: possible issues and concerns. *Am Pharm Rev*. 2011; Available from <https://www.americanpharmaceuticalreview.com/Featured-Articles/37021-Freeze-Drying-Protein-Formulations-above-their-Collapse-Temperatures-Possible-Issues-and-Concerns/> [Accessed 29<sup>th</sup> November 2020].
- Pikal MJ. Freeze-drying of proteins. Part I: Process Design. *Biochem Pharmacol*. 1990;3:18–28.
- Pikal MJ. Use of laboratory data in freeze drying process design: heat and mass transfer coefficients and the computer simulation of freeze drying. *J Parenter Sci Technol*. 1985;39:115–38.
- Scutella B, Bourles E. Development of a freeze-drying cycle via design space approach: a case study on vaccines. *Pharm Dev Technol*. 2020;25(10):1302–13.
- Pisano R, Fissore D, Barresi AA. Freeze-drying cycle optimization using model predictive control techniques. *Ind Eng Chem Res*. 2011;50(12):7363–79.
- Shivkumar G, Kazarin PS, Strongrich AD, Alexeenko AA. LyoPRONTO: an open-source lyophilization process optimization tool. *PharmSciTech*. 2019;20:238.
- Wegiel L. Primary drying optimization using a three-dimensional design space. Presented at CPPR Conference Freeze Drying of Pharmaceuticals and Biologicals Conference. Germany: Garmisch-Partenkirchen; 2014. p. 23–6.
- Nail SL, Searles JM. Elements of quality by design in development and scale-up of freeze-dried parenterals. *BioPharm Int*. 2008;21(1):44–52.
- Patel AM, Chaudhuri S, Pikal MJ. Choked flow and importance of Mach I in freeze-drying process design. *Chem Eng Sci*. 2010;65(21):5716–27.
- Pikal MJ, Pande P, Bogner R, Sane P, Mudhivarthi V, Sharma P. Impact of natural variations in freeze-drying parameters on product temperature history: application of quasi steady-state heat and mass transfer and simple statistics. *PharmSciTech*. 2018;19(7):2828–42.
- Pikal MJ, Bogner R, Mudhivarthi V, Sharma P, Sane P. Freeze-drying process development and scale-up: scale-up of edge vial versus center vial heat transfer coefficients, Kv. *J Pharm Sci*. 2016;105(11):3333–43.
- Gieseler H, Kessler WJ, Finson MF, Davis SJ, Mulhall PA, Bons V, Debo DJ, Pikal MJ. Evaluation of tunable diode laser absorption spectroscopy for in-process water vapor mass flux measurements during freeze-drying. *J Pharm Sci*. 2007;96(7):1776–93.
- Schneid S, Gieseler H, Kessler W, Pikal MJ. Position dependent vial heat transfer coefficient: a comparison of tunable diode laser absorption spectroscopy and gravimetric measurements. Presented at CPPR Freeze-Drying of Pharmaceuticals and Biologicals. Germany: Garmisch-Partenkirchen; 2006. p. 3–6.
- Kuu WY, Nail SL, Sacha G. Rapid determination of vial heat transfer parameters using tunable diode laser absorption spectroscopy (TDLAS) in response to step-changes in pressure set-point during freeze-drying. *J Pharm Sci*. 2009;98(3):1136–54.
- Schneid SC, Gieseler H, Kessler WJ, Pikal MJ. Non-invasive product temperature determination during primary drying using tunable diode laser absorption spectroscopy. *J Pharm Sci*. 2009;98(9):3401–18.
- Kuu WY, O'Bryan KR, Hardwick L, Paul TW. Product mass transfer resistance directly determined during freeze-drying cycle runs using tunable diode laser absorption spectroscopy (TDLAS) and pore diffusion model. *Pharm Dev Technol*. 2011;16(4):343–57.
- Bogner R. Factors that influence product resistance and methods to measure product resistance. SP Scientific Webinar, 2020 March 23<sup>rd</sup>. Available from: <https://www.spscientific.com/Webinars/Archives/> [Accessed 10th October 2020].
- Sharma P, Kessler WJ, Bogner R, Thakur M, Pikal MJ. Applications of the tunable diode laser absorption spectroscopy: in-process estimation of primary drying heterogeneity and product temperature during lyophilization. *J Pharm Sci*. 2019;108(1):416–30.
- Tang X, Nail SL, Pikal MJ. Freeze-drying process design by manometric temperature measurements: design of a smart freeze-dryer. *Pharm Res*. 2005;22(4):685–700.
- Pikal MJ, Roy ML, Shah S. Mass and heat transfer in vial freeze-drying of pharmaceuticals: role of the vial. *J Pharm Sci*. 1984;73(9):1224–37.
- Engineering ToolBox, (2004). Ice - thermal properties. [online] Available at: [https://www.engineeringtoolbox.com/ice-thermal-properties-d\\_576.html](https://www.engineeringtoolbox.com/ice-thermal-properties-d_576.html) [Accessed 27 July 2021].
- Jancso G, Pupezin J, Van Hook WA. Vapor pressure of ice between+ 10-2 and-1020. *J Phys Chem*. 1970;74(15):2984–9.
- Patel SM, Nail SL, Pikal MJ, Geidobler R, Winter G, Hawe A, Davagnino J, Gupta SR. Lyophilized drug product cake appearance: what is acceptable? *JPharmSci*. 2017;106:1706–21.

**Publisher's Note** Springer Nature remains neutral with regard to jurisdictional claims in published maps and institutional affiliations.